Enhancing the estimation of continental-scale snow water equivalent by assimilating MODIS snow cover with the ensemble Kalman filter

Hua Su,[1] Zong-Liang Yang,[1] Guo-Yue Niu,[1] and Robert E. Dickinson[2]

Received 28 July 2007; revised 30 October 2007; accepted 10 January 2008; published 30 April 2008.

[1] High-quality continental-scale snow water equivalent (SWE) data sets are generally not available, although they are important for climate research and water resources management. This study investigates the feasibility of a framework for developing such needed data sets over North America, through the ensemble Kalman filter (EnKF) approach, which assimilates the snow cover fraction observed by the Moderate Resolution Imaging Spectroradiometer (MODIS) into the Community Land Model (CLM). We use meteorological forcing from the Global Land Data Assimilation System (GLDAS) to drive the CLM and apply a snow density-based observation operator. This new operator is able to fit the observed seasonally varying relationship between the snow cover fraction and the snow depth. Surface measurements from Canada and the Advanced Microwave Scanning Radiometer-Earth Observing System (AMSR-E) estimates (in particular regions) are used to evaluate the assimilation results. The filter performance, including its ensemble statistics in different landscapes and climatic zones, is interpreted. Compared to the open loop, the EnKF method more accurately simulates the seasonal variability of SWE and reduces the uncertainties in the ensemble spread. Different simulations are also compared with spatially distributed climatological statistics from a re-gridded data set, which shows that the SWE estimates from the EnKF are most improved in the mountainous west, the northern Great Plains, and the west and east coast regions. Limitations of the assimilation system are analyzed, and the domain-wide innovation mean and normalized innovation variance are assessed, yielding valuable insights (e.g., about the misrepresentation of filter parameters) as to implementing the EnKF method for large-scale snow properties estimation.

Citation: Su, H., Z.-L. Yang, G.-Y. Niu, and R. E. Dickinson (2008), Enhancing the estimation of continental-scale snow water equivalent by assimilating MODIS snow cover with the ensemble Kalman filter, *J. Geophys. Res.*, *113*, D08120, doi:10.1029/2007JD009232.

1. Introduction

[2] Snow is a very important component of the climate system which controls surface energy and water balances. Its high albedo, low thermal conductivity and properties of surface water storage impact regional to global climate, as has been documented in numerous observational and modeling studies [e.g., *Barnett et al.*, 1989; *Yang et al.*, 2001; *Gong et al.*, 2003].

[3] The various properties characterizing snow are highly variable and so have to be determined as dynamically active components of climate. These include the snow water equivalent (SWE), density, and show cover fraction (SCF). However, on large spatial scales the properties of snow are not easily quantified either from modeling or observations. For example, station based snow measurements often lack spatial representativeness, especially in regions where the topography, vegetation and overlaying atmosphere produce considerable heterogeneity of the snowpack distribution [*Liston*, 2004]. In recent decades SWE and snow depth products have been available from passive microwave sensors (e.g., the Advanced Microwave Scanning Radiometer-Earth Observing System (AMSR-E)). Nevertheless, since the microwave signature of snowpack depends on a number of varying features (e.g., snow grain size, density, liquid water content, vegetation, etc), direct estimation (e.g., linear regression) of snow parameters that does not include these dynamic properties can be plagued by complicated errors [*Grody and Basist*, 1996; *Foster et al.*, 2005; *Dong et al.*, 2005]. In addition, snow estimation from land surface models (LSMs) can have large uncertainties partly owing to their imperfect parameterizations of snow dynamics and the errors in their meteorological forcing. Since neither observations nor LSMs alone are capable of providing adequate

[1]Department of Geological Sciences, The John A. and Katherine G. Jackson School of Geosciences, University of Texas at Austin, Austin, Texas, USA.

[2]Department of Earth and Atmospheric Sciences, Georgia Institute of Technology, Atlanta, Georgia, USA.

0148-0227/08/2007JD009232$09.00

information about the time space variability of continental snow properties, it becomes necessary to combine their information, as achievable through the technology of land surface data assimilation [e.g., *McLaughlin*, 2002; *Houser et al.*, 1998; *Reichle et al.*, 2002; *Margulis et al.*, 2002; *Crow*, 2003]. Such assimilation can effectively reduce estimation uncertainties through optimally combining the information from both LSMs and observations.

[4] A number of studies have initially applied data assimilation methods for deriving snow properties (e.g., SWE) [e.g., *Rodell and Houser*, 2004; *Slater and Clark*, 2006; *Dong et al.*, 2007; *Durand and Margulis*, 2006, 2007]. Among these studies the ensemble Kalman filter (EnKF) has been used to combine the observed SCF information with the model simulated SWE [e.g., *Andreadis and Lettenmaier*, 2006; *Clark et al.*, 2006]. The SWE, a prognostic variable derived from the snow mass balance, has been optimally updated through its correlative relationship with other more readily observed quantities (e.g., SCF). However, most of these studies were confined to small river basins or plot scales, and few have addressed continental or hemispheric applications where the snow effects on the atmospheric circulation may be pronounced and where the simulation and observational uncertainties of snow properties may depend on different landscape properties and climate zones. Thus, more optimal methods of estimation on these scales are needed. Further, only limited (some very simple) snow physical models and observational functions were involved in previous studies, and the performance of the data assimilation was inadequately evaluated for operational application. Therefore the feasibility of data assimilation methods for the retrieval of such properties on a large scale has not yet been decisively demonstrated.

[5] The purpose of this paper is to assess the feasibility of the EnKF methodology and a new observational operator for the retrieval of SWE on a continental scale. It demonstrates that the SCF as measured by the Moderate Resolution Imaging Spectroradiometer (MODIS) instrument can be assimilated into continental SWE fields simulated by a highly complex LSM, i.e., the National Center for Atmosphere Research (NCAR) Community Land Model (CLM). Section 2 gives a brief description of the EnKF, the CLM, and a recently developed SCF observational operator. Data sets and experiments are discussed in section 3. The results analyses are given in section 4. Section 5 discusses limitations of the proposed method, with concluding remarks in section 6.

2. Methodology

[6] The EnKF based snow data assimilation system used in this paper has two essential components: (1) an LSM (including its snow model) that evolves related state variables in an ensemble approach and provides background error statistics; (2) the Kalman filter updating scheme that combines the physical simulations with observations using an observational function.

2.1. LSM

[7] The CLM [e.g., *Bonan et al.*, 2002; *Oleson et al.*, 2004] numerically simulates energy, momentum and water exchanges between the land surface and the overlying atmosphere at each computational grid. It employs 10 soil layers to resolve soil moisture and temperature dynamics and uses plant functional types (PFTs) to represent subgrid vegetation heterogeneity. The CLM snow model simulates a snowpack with multilayers (1–5 layers) depending on its thickness, and accounts for processes such as liquid water retention, diurnal cycling of thawing-freezing, snowmelting, and surface frost and sublimation. Heat and water are transported between its adjacent snow layers, also between its top layer and the overlying canopy and/or the atmosphere. Snow layers may be combined or divided every time step to ensure a realistic representation of snow physics and numerical stability. The grid averaged albedo is area weighted using a snow cover fraction. The CLM also explicitly incorporates densification processes (e.g., destructive or equitemperature metamorphism, compaction by snow overburden, and melt metamorphism) following *Anderson* [1976], for calculating snow density of each snow layer. This multilayer approach is found to significantly enhance the simulation quality, correcting the previously underestimated snow mass and early time of melting that is obtained in a single layer model [*Yang and Niu*, 2003].

[8] The SWE propagation equation in the CLM can be summarized as follows:

$$x_t = x_{t-1} + (P_t - E_t - M_t)dt \tag{1}$$

where x_t and x_{t-1} denote the SWE in a subgrid tile of a grid at time step t and $t-1$, respectively. P_t represents the solid precipitation provided by measurements, E_t represents the loss of snow owing to sublimation and evaporation, and M_t represents the melting of snow. The latter two quantities are calculated from the model. By adding together layers, the subgrid tile total SWE can be obtained as:

$$x_t = \sum_{i=0}^{snl+1} \left(w_{ice,i} + w_{liq,i}\right) \tag{2}$$

where $w_{ice,i}$ and $w_{liq,i}$ denote solid and liquid water mass in layer i, and snl denotes the number of layers. Each of these terms has its own mass balance equation similar to (1).

2.2. EnKF and Its Implementation

[9] The EnKF was first introduced by *Evensen* [1994] as a Monte Carlo approach to accomplish the Kalman filter updating scheme in numerical modeling systems. It is also related to the theory of Stochastic Dynamic Prediction [*Epstein*, 1969]. Detailed descriptions and discussions of this method in various contexts are available in the literature [e.g., *Evensen*, 1994, 2003; *Reichle et al.*, 2002; *Hamill*, 2006].

[10] Using the model physical configuration described in 2.1, the EnKF is implemented as follows: (1) each sample (i.e., ensemble member) of model state variables is propagated at every time step using prognostic equations like equation (1); these simulations are driven by perturbed meteorological forcing data (the method of sampling forcing is introduced in section 3); and (2) each sample of the LSM

forecast variables is updated (e.g., SWE in this study) using equation (3):

$$x_{i,t}^{j\,\prime} = x_{i,t}^{j} + K_t\left(y_t - H\left(x_{i,t}^{j}\right) + v_t^{i}\right) \tag{3}$$

where $x_{i,t}^{j\prime}$ denotes the filter updated states (e.g., SWE), $x_{i,t}^{j}$ the model simulated states, i the ensemble index, j the tile index in a given grid, y_t the observation in that grid (SCF in this study), and H the observational operator (to be described subsequently). v_t^i is randomly drawn from a Gaussian distribution (with zero mean and the variance equal to R_t as described below) to ensure an adequate spread of the analysis ensemble members [*Burgers et al.*, 1998].

[11] The K_t in equation (3), i.e., the "Kalman gain", takes the form of:

$$K_t = P_t^b H^T \left(H P_t^b H^T + R_t\right)^{-1} \tag{4}$$

where P_t^b represents the error covariance of simulated ensembles; R_t, the error covariance of observed SCF. The latter is a prescribed value in this study. The model state $x_{i,t}^j$ is a subgrid tile based value, while the observational statistic y_t (SCF) is defined at a grid. The model is compared with observation using $H(x_{i,t}^j)$, the summation of model predicted SCF over all tiles in the specified grid:

$$H\left(x_{i,t}^{j}\right) = \sum_{e=1}^{n} h\left(x_{i,t}^{e}\right) \tag{5}$$

where e loops all the tiles in the grid and $h(x_{i,t}^e)$ denotes the observational operator at each tile weighted by the tile area. It should be emphasized that the above implementation does not directly assimilate SWE measurements nor does it directly update the CLM simulated SCF. Instead the implementation updates the CLM simulated SWE with SCF observations, which requires an observation function linking the state variable SWE and the MODIS observed SCF as described in section 2.3.

[12] The updated SWE or $x_{i,t}^{j\prime}$ in equation (3) represents the total snow mass for the entire snowpack, which must be disaggregated into ice and liquid parts for each of the layers according to (2). A simple rule is designed for this allocation. Snow mass is always added or subtracted in the layers starting from the top, and the ratio between solid and liquid water components is kept the same after each allocation. The total snow mass and energy are conserved as the layers are separated or combined, and the procedure follows the existing parameterization in the snow layering scheme [*Oleson et al.*, 2004]. The snow depth in each layer is also updated accordingly. In CLM the snow density is calculated from the snow water equivalent and snow depth, therefore it is updated by the above method.

2.3. Observational Operator

[13] A snow depletion curve (SDC) that parameterizes the relationship between regional averaged SWE and SCF has been used to optimize SWE estimates in recent ensemble based data assimilation experiments [e.g., *Andreadis and Lettenmaier*, 2006; *Clark et al.*, 2006]. Its basic philosophy is that the accumulation or ablation of the unevenly distributed snow determines both SWE and SCF such that both are highly correlated [*Yang et al.*, 1997; *Luce et al.*, 1999; *Luce and Tarboton*, 2004; *Liston*, 2004]. Accordingly, any observed SCF information should contribute to the estimation of SWE.

[14] A new SCF parameterization has been developed by *Niu and Yang* [2007] using the snowpack density to account for the large-scale depletion pattern and its temporal variability. This SCF scheme, which is used in this study to transfer observational information into the CLM, takes the following mathematical form:

$$SCF = \tanh\left(\frac{h_{sno}}{2.5 z_0 (\rho_{sno}/\rho_{new})^{\alpha}}\right) \tag{6}$$

where SCF is the snow cover fraction, h_{sno} and z_0 are the spatially averaged snow depth (or rewritten to be a function of SWE and snow density) and the ground roughness length, respectively. ρ_{new} is a prescribed fresh snow density with adjustable values depending on local conditions. ρ_{sno} is the model calculated snow density. The curve shape parameter α is tunable and assumed to be controlled by several factors including scale and, hypothetically, the grid-specific physiographic properties. The value 2.5 in equation (6) is itself tunable, but it is here assumed to be a constant for simplicity.

[15] The snow depth and snow cover relationship (equation (6)) differs from any of the parameterizations reviewed by *Liston* [2004]. Instead of one static curve for the entire snow season, it provides a family of snow depletion curves with each such curve representing a nonlinear relationship between SCF and snow depth characterized by a unique value of snowpack density (Figure 1). Further, this SCF operator accommodates the multilayer structure of CLM snow model by using the layer integrated snow density in the equation (6). *Niu and Yang* [2007] evaluated the validity of this seasonally varying SCF scheme using long-term (1979–1996) ground based data of SWE and snow depth in North America [*Brown et al.*, 2003] and satellite observed monthly SCF from AVHRR. Equation (6) performs reasonably well in terms of reconstructing the relationship between SCF and snow depth in large river basins in North America.

[16] To apply equation (6) for data assimilation, we need to calibrate ρ_{new} and α on the basis of field measurements or other high-quality data sets at hand. This study sets ρ_{new} to 100 kg/m^3 [*Dingman*, 2002] for each grid in the model domain. We use gridded North America snow data sets (1979–1996) [*Brown*, 2003] and AVHRR monthly SCF data to calibrate the shape parameter α. The reason to use the AVHRR SCF data set is that it covers the same time period as the data in the work of *Brown et al.* [2003]. These data sets are regridded to 1° by 1° resolution, the resolution used for the off-line model. An optimal α is obtained by requiring the SCF derived from equation (6) to best fit the AVHRR observed SCF in a least mean square error sense. The Genetic Algorithm (GA) is used to efficiently search for this optimal parameter. We account for the region-specific variability of α by considering three landscape categories: (1) flat regions with low standing vegetation (e.g., the prairie in the northern Great Plains); (2) flat regions with highstanding vegetation (e.g., the boreal forest of Canada)

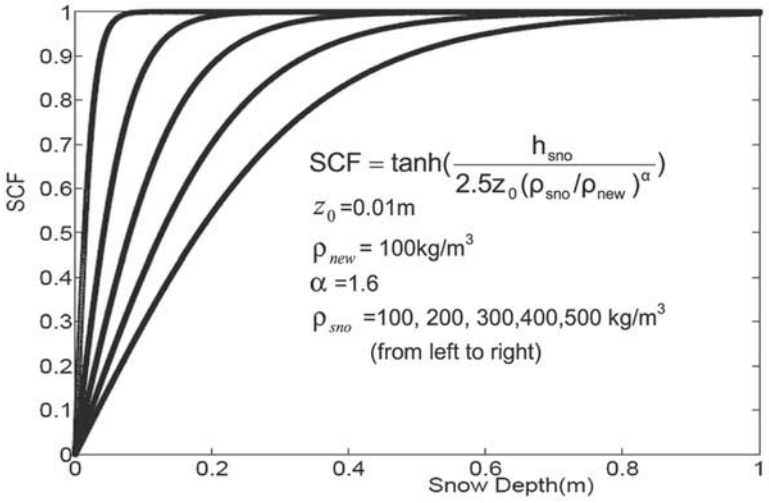

Figure 1. SCF parameterization using snow density. Each curve represents a different snow density in equation (6).

and (3) mountainous regions (e.g., the Rocky Mountains). This approach to representing heterogeneity of SDC is comparable to that of *Liston* [2004], which used a statistical distribution to characterize SDC and retrieve related parameters (e.g., CV in the work of *Liston* [2004]) on the basis of the physiographic properties of a geographic region to represent.

[17] We have selected three regions in North America to represent the above landscape categories, each large enough to retrieve the optimal value of α. The calibrated α (using observations from 1979 to 1993) and correlation coefficient between reconstructed and observed SCF in the validation period (using observations from 1994–1996) are given in Table 1. Table 1 shows that α is slightly less than one for the flat and low vegetation region, greater than two for the flat and high vegetation region, and in between over mountainous regions.

3. Experimental Setup and Data Sets

[18] We use near surface meteorological forcing variables from the Global Land Data Assimilation System (GLDAS) at $1^\circ \times 1^\circ$ resolution [*Rodell et al.*, 2004] to drive CLM. The GLDAS forcing data are observationally derived fields including precipitation, air temperature, air pressure, specific humidity, shortwave and longwave radiation. The vegetation and soil parameters from finer resolution raw data of CLM2.0 as used in previous studies [*Bonan et al.*, 2002; *Niu et al.*, 2005] are aggregated. CLM is run from January 2002 to June 2004, spanning the time period during which the MODIS retrieved SCF is available.

[19] The GLDAS precipitation and temperature fields are perturbed in order to account for uncertainties in these model inputs to the snow dynamics. The samples of precipitation forcing are derived by multiplying the GLDAS values by spatially correlated lognormal random fields (with zero mean and unit variance), as described in the work of *Nijssen and Lettenmaier* [2004]. The e-folding scale of horizontal error correlations are assumed to be 1° in latitude/longitude coordinates, to provide the spatial covariance of forcing uncertainties. The relative error is defined at 50% in the lognormal distribution approach. Temperature ensembles are produced in the same way, except that typical normal random fields are applied to mimic true uncertainties, with zero mean and 3°C standard deviation. The ensemble size is set to 25, a compromise between computational affordability in the large land assimilation system and the filter effectiveness. Previous studies [e.g., *Reichle et al.*, 2002; *Andreadis and Lettenmaier*, 2006] showed reasonable performance for the EnKF with this ensemble size.

[20] We assimilate the MODIS observed snow cover fraction into the CLM. MODIS uses 36 spectral bands to retrieve land surface properties. Its snow mapping algorithm detects land snow fraction using a normalized difference snow index (NDSI) [*Hall et al.*, 1995], and has the ability to distinguish between snow and cloud [*Hall et al.*, 2002]. The spatial resolution of SCF data from MODIS can be as high as 500 m but the product applied in this research is MOD10C1 with 0.05° resolution [*Hall et al.*, 2002]. We determine from the 0.05°Cells, a weighted average at 1° resolution using the CMG confidence indices [*Hall et al.*, 2002], assuming that the raw data SCF is unchanged by cloud obscuration. A threshold of 50% for the cloud cover is used to determine whether or not the SCF observation is used in the corresponding grid. This value is reasonable in that it does not have large negative effects on the filter performance compared to a stricter criteria, while rendering the system a relative increase in the SCF data frequency. The model is spun up to November 2002, and after that the MODIS SCF data sets are assimilated.

[21] The MODIS SCF has errors whose standard deviation varies seasonally and geographically. Accurate charac-

Table 1. Calibrated Parameter α Used in Observation Operator for Different Land Types

	Flat and Low Vegetation	Mountainous Regions	Flat and High Vegetation
Optimized α	0.98	1.69	2.21
Correlation coefficient R	0.92	0.82	0.96

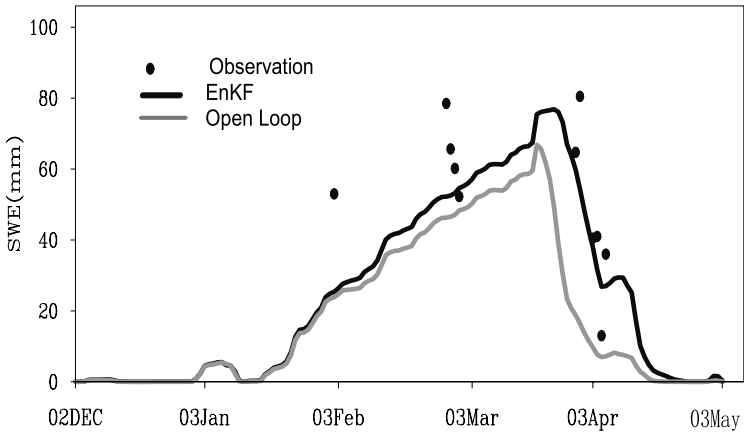

Figure 2. Comparison of regional averaged SWE (52°–54°N, 112°–114°W in 2002–2003) from simulation results and ground observations.

terization of the MODIS SCF error structure is beyond the scope of this study. An extensive literature search [e.g., *Klein and Barnett*, 2003; *Simic et al.*, 2004; *Brubaker et al.*, 2005; *Hall and Riggs*, 2007] indicates that it is fairly reasonable to assume the MODIS error at 10% in this particular study. Using this simple, stationary error criteria is also consistent with previous research [e.g., *Andreadis and Lettenmaier*, 2006]. To account for parameter errors, a Gaussian error distribution with zero mean and 10% (based on nominal value in Table 1) standard deviation is prescribed for α in equation (6).

[22] High quality, spatially distributed ground SWE data at the continental scale are generally not available as independent data sets for validation. Furthermore, since the snow density is simulated to be a time-dependent variable as considered in equation (6), the abundant measurements of snow depth across North America (e.g., the NOAA Coop measurements) may not be directly applied as a benchmark for evaluating the SWE. Another limitation is the requirement that GLDAS forcing data overlap with MODIS observations, precluding their use for long-term simulations.

[23] On the basis of these considerations, two independent observational sources are used to evaluate the assimilated continental-scale SWE fields. The first source is the ground measurements in Canada [*Meteorological Service of Canada*, 2000] which contain snow course surveyed SWE data over recent decades. The Canada snow course data are mainly located in river basins in southern Canada [*Meteorological Service of Canada*, 2000; *Brown et al.*, 2003] encompassing different topographic and vegetative types. The measurements from winter 2002 to summer 2003 (overlapping with the CLM integration period) are scattered in western mountainous regions and southern flat regions, with a relatively small portion of area in the central southern prairie region. The other source is AMSR-E derived SWE data. AMSR-E (flown on board the NASA Aqua satellite) is a passive microwave radiometer with a wide range of frequencies (from 6.9–89 GHz), which can provide spatially and temporally continuous SWE estimation with adequate resolution for global analyses. These SWE estimates may have large errors in mountainous regions, forests, and where the snow is wet [e.g., *Dong et al.*, 2005; *Foster et al.*, 2005]. Under certain circumstances, e.g., for low vegetation flat regions where snow is dry and shallow, the snow grain size and snow density assumed in the retrieval algorithm are relatively reliable (e.g., the northern Great Plains), and the passive microwave retrieved SWE can be relatively accurate [*Brubaker et al.*, 2001; *Mote et al.*, 2003; *Foster et al.*, 2005].

4. Results

4.1. Initial Evaluation of the Assimilated SWE Data Set

4.1.1. Comparison With Ground Observations

[24] Distributed observations in the Canadian prairie region are limited, but they are still suitable for our evaluation. Figure 2 shows the interstation averaged measurements and their simulation counterparts within the region of 52°–54°N, 112°–114° in the 2002–2003 cold season. This comparison is rather representative in our assessing the assimilation quality for several reasons. First, it illustrates the relatively low frequency of ground observations, though the accumulation and melting stages are clearly displayed. Second, it represents some typical benefits through incorporating the SCF information into the CLM simulation in broad prairie regions. Figure 2 shows that the assimilated SWE values at the peak and melting stage are elevated to value closer to the observations. The extent to which the SWE is adjusted changes from place to place, determined by the weighting of model forecasted SCF and MODIS observed SCF according to the ensemble error statistics. In this particular case, the CLM predicted SCF is lower than that from the MODIS observations, and the filter partially corrected this difference during the assimilation cycles. Although only limited ground validation are provided here, it is argued that these analyses are consistent with our purpose, which is to obtain a qualitative assessment on the proposed methodology.

4.1.2. Comparison With Passive Microwave Sensor Retrieved Data in Selected Regions

[25] Global SWE estimates from AMSR-E are available for the period of the CLM simulations in selected regions in North America. In the midlatitude flat and low vegetation

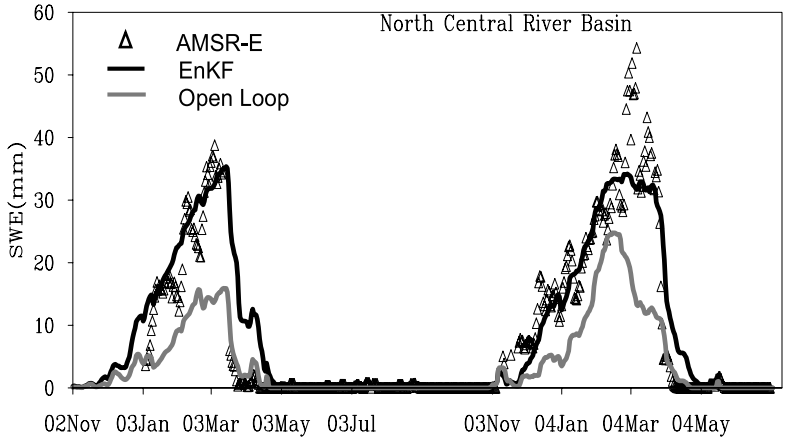

Figure 3. Comparisons among daily basin-averaged SWE estimations in North Central River Basin. A five-day moving average is used on AMSR-E data to filter out the high-frequency fluctuations in the original AMSR-E daily data. This high-frequency component is assumed to be caused by the incomplete coverage of the AMSR footprints in this region, which is frequently present during the simulation period. Same filter is used in AMSR data in Figure 4.

covered regions with a shallow snowpack, such as the Missouri River Basin and the North Central River Basin, AMSR-E derived daily SWE products can be utilized for assessing assimilation results. The comparisons are shown in Figures 3 and 4. In each plot the daily time series of basin averaged snow water equivalent estimates are displayed, representing the EnKF assimilation run, the open-loop run (without assimilation) and the AMSR-E estimation, respectively. The figures indicate that the SCF assimilation significantly adjusts the snow estimation in these two basins and provides results more like the AMSR-E estimates. During December to February when the snow is likely to be dry in those regions, the AMSR-E retrieved SWE should have less uncertainty induced by liquid water content [*Tedesco et al.*, 2006]. During this time, the EnKF simulations better agree with satellite observations than over the melting period of March and April. Some new snow retrieval algorithms are currently under development for more accurately inverting or assimilating the passive microwave signals [e.g., *Markus et al.*, 2006; *Durand and Margulis*, 2006]. The above results may be further evaluated when those enhanced SWE estimations from space-borne sensors are available.

4.1.3. Spatial Patterns Evaluation

[26] A ground based SWE regridded data set from *Brown et al.* [2003] is used to further assess the distribution of EnKF assimilated SWE. Its climatological monthly mean values and the associated anomalies facilitate us to interpret the difference between the model above (open loop) and EnKF simulations. Figure 5 shows the spatial distribution of monthly mean SWE (February 2003) from different simulations, also the climatological mean (comparisons in other months have similar results). It is clear that in many regions the EnKF results and the climatology are more similar to each other than with the open loop, particularly in the northern Great Plains, the Midwest mountainous regions, west costal regions, and part of the east costal regions. However, the EnKF simulation has a high bias in the boreal forests, which may reflect the forest effects on MODIS SCF data, or the systematic error in the meteorological forcing.

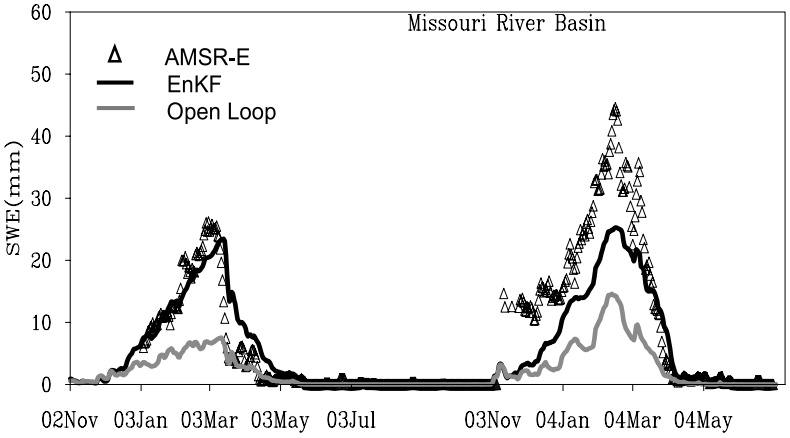

Figure 4. Comparisons among daily basin-averaged SWE estimations in the Missouri River Basin.

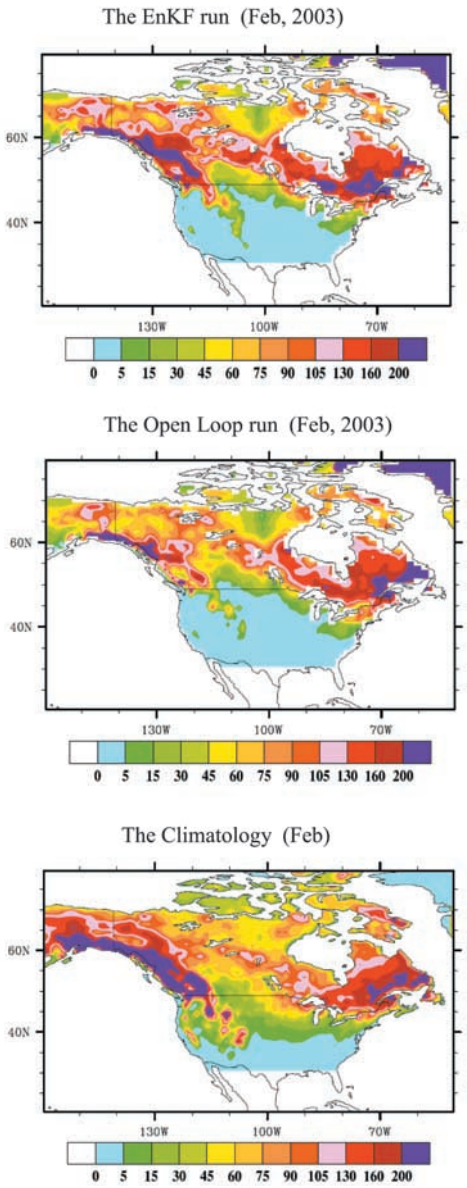

Figure 5. The spatial distribution of the monthly averaged SWE (mm) in February from the EnKF and open loop simulations, the climatology from reanalysis data set, and the AMSR data set.

[27] Figure 6 shows the climatological standard deviation of SWE (February) as derived from the multiyear reanalysis data set, and the absolute difference between each simulation (February 2003) and the climatology. It demonstrates that in most of the regions where the EnKF and the climatology are in better agreement, their differences are within the range of interannual variability. Figure 7 further supports this conclusion using a temporal comparison of monthly mean SWE (from November 2002 to June 2003) in three small representative places within those regions summarized above. The error bars associated with the climatological mean denotes the standard deviations of monthly SWE. During the majority of the snow season (e.g., from January to March), the EnKF simulated monthly mean values are usually confined within the error bar. In contrast, the open loop simulations are often outside of the standard deviation range. Specifically in the first region (41°–42°N, 75°–80°W) the difference between the open loop and the mean is nearly twice a standard deviation, which suggests the erroneousness of the open loop simulation there. The above spatial evaluation takes an indirect approach because the multiyear data used to construct climatological statistics do not cover our simulation periods. However, it should be meaningful, partly because

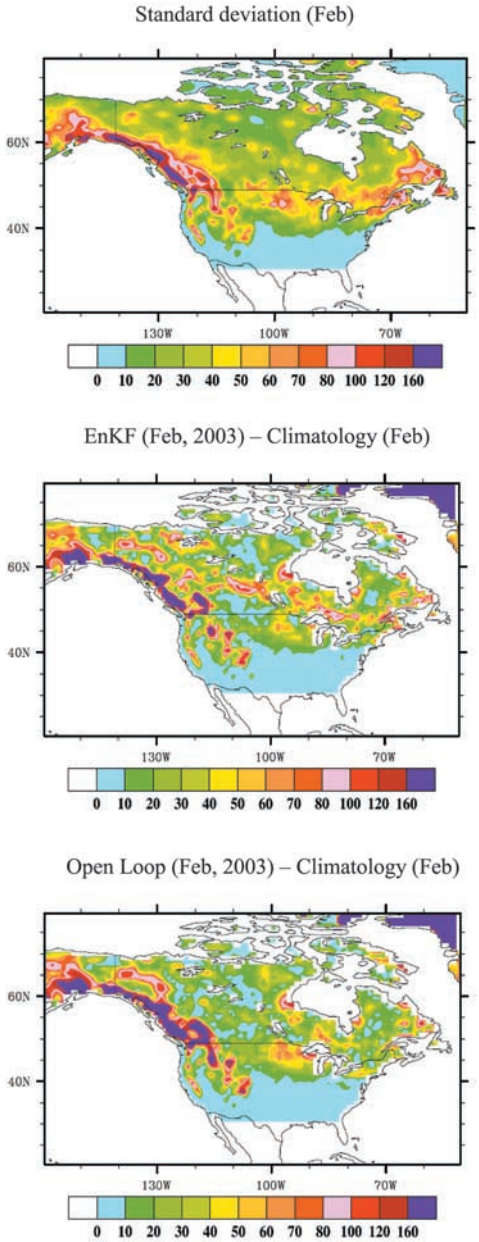

Figure 6. The spatial distribution of SWE standard deviation (mm) in February derived from the reanalysis data set, the absolute value of monthly mean (February) difference (mm) between the EnKF and climatology, also the difference (mm) between the open loop and climatology.

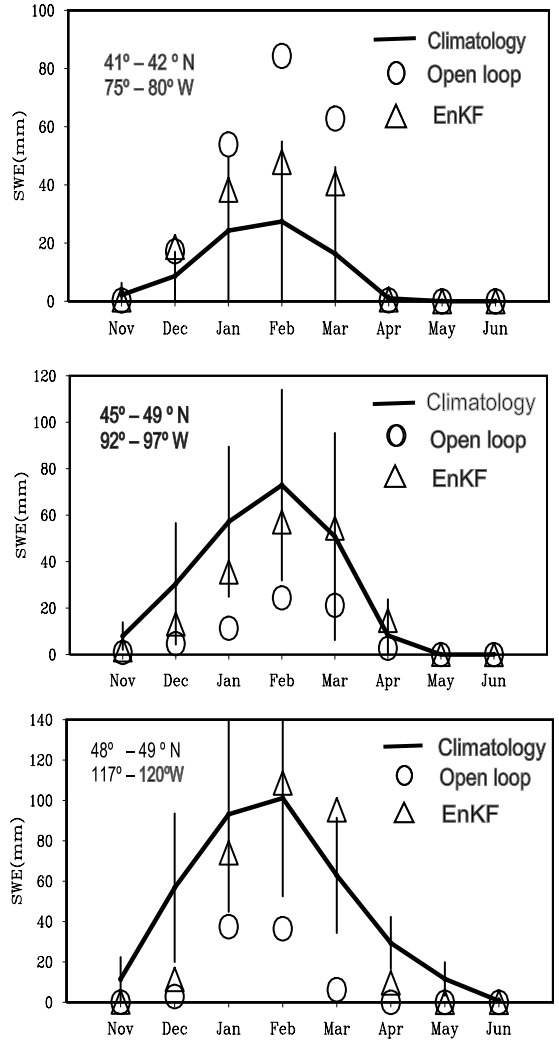

Figure 7. Comparison of the EnKF and open loop simulated monthly mean SWE with reanalysis derived climatological mean from November 2002 to June 2003 in three rectangular regions. The error bar (vertical line) is given for each climatological mean value, which stands for the standard deviation (interannual variability) of each month.

of the relative stability of climatological mean and standard deviation of large-scale SWE.

4.2. Assessing the Behavior of Ensemble Filtering in Large-Scale Snow Assimilation

[28] The ensemble simulations of SWE at the CLM grid test sites with different land surface properties and climatic scenarios are presented in Figures 8, 9, and 10. Figure 8 shows by the middle-latitude prairie grid that the model simulations have large spreads in both accumulation and melting periods. This variability is markedly reduced in the data assimilation run, especially in the melting season. Apparently, the GLDAS forcing terms do not fully constrain the timing of melting compared to the EnKF. Meanwhile the decrease in the EnKF ensemble variance demonstrates that the EnKF algorithm is implemented properly in this simulation.

[29] Typical simulation results in boreal forest regions are shown in Figure 9. Similar to those displayed in Figure 8, the ensemble uncertainties are reduced in the EnKF run. However, the effect of altering the peak SWE is not as significant as that shown in Figure 8. These areas are covered by large extent of snow of a longer duration than that of the prairie regions (where the snow cover is usually ephemeral), so it is easier for the model simulated SCF to agree with MODIS observation, making the filter update more smooth.

[30] The filter characteristics for a mountainous grid in Colorado (Figure 10) appear to be similar to those in Figures 8 and 9. However, it differs from the other two in that the timing of snowmelt is largely altered in the EnKF simulation owing to the incremental information obtained from MODIS. Since it is a mountainous grid, this SWE updating is possibly useful for local water resources management.

5. Discussion

[31] The EnKF snow simulation system has several limitations. The snow model used and the other physical representations of land surface processes are not perfect. For example, although it has detailed vertical processes, the model does not adequately represent horizontal mechanisms such as the bare soil effects and heat advection across snow patches. Both such limitations in the model physics and the systematic error in the meteorological forcing may result in a bias in the estimate of SWE and other quantities, which would make the filter system suboptimal. The innovation mean, i.e., the mean of the difference between the observation and the model simulated corresponding variable (SCF in this study), can be used to evaluate the bias in the data assimilation system. If the system is bias free and purely linear, the innovation mean should be zero [*Dee*, 1995]. The domain-wide innovation mean distribution for the winter season of 2002–3003 is shown in Figure 11. It shows that this statistic is significantly larger than its theoretical expectation, i.e., zero, in some grids in the western United States and the northern Great Plains, indicating the model system has negative bias there. In contrast, its value is lower than zero in the northeast of North America, representing positive bias there. The bias in the snow assimilation system might be reduced by following the "cdf matching" method applied in the work of *Reichle and Koster* [2004], in which the satellite observations are scaled to agree with the model simulated climatology (soil moisture in their paper). Other potential approaches may include enhanced representation of model parameters and structures (system identification) in the data assimilation framework.

[32] Determining the covariance of forcing errors is another important issue in land data assimilation systems [*Reichle and Koster*, 2003; *Crow and Loon*, 2006]. The forcing error variances largely dictate the ensemble evolving path and the magnitude of the EnKF updates. The mean of normalized innovation variance can be used to detect the misrepresentation of model error in the data assimilation system, as defined below:

$$\varphi = E\left[\frac{v^T v}{HP_t^b H^T + R_t}\right] \tag{7}$$

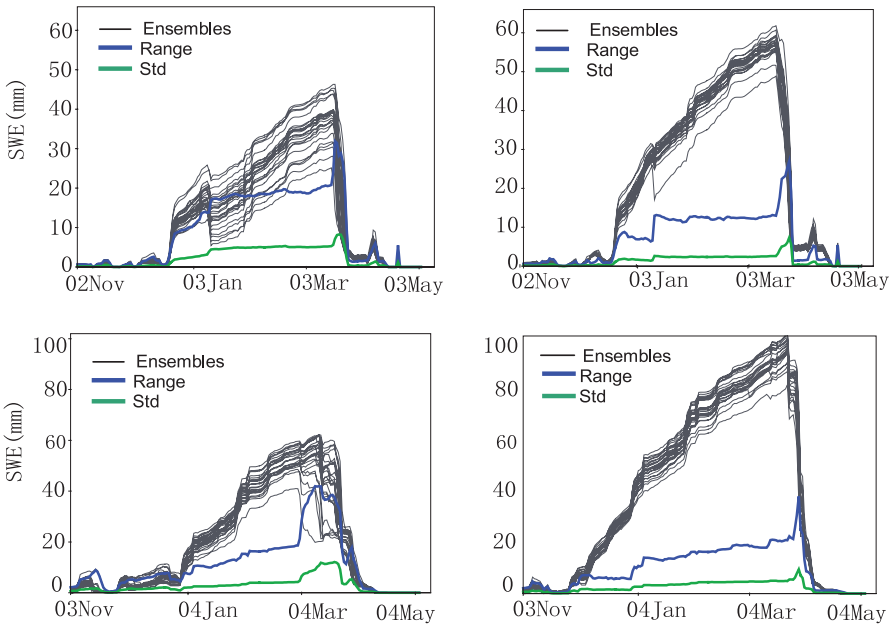

Figure 8. Ensemble simulations of SWE and their error statistics at a grid in the prairie region. Left panels show the open loop run; right panels show the EnKF run. Upper panels are for 2002–2003; lower panels are for 2003–2004. Ensemble simulations are represented by gray curves, the range (difference between the maximal ensemble value and the minimal ensemble value) of ensemble by the blue curve, and the standard deviation of ensemble by the green curve.

where v represents the average of innovation over the ensemble members, and $E[]$ represents the temporal mean.

[33] If the EnKF is used with optimal statistical conditions (e.g., linear models and observational operators, and additive Gaussian errors), and the model errors are perfectly represented by the ensemble statistics, then the mean of the normalized variance of the innovation should = 1.0 [*Dee*, 1995]. The spatial distribution of the mean of the normalized innovation variance for the winter season in 2002–2003 is shown in Figure 12. Its value is significantly larger than this theoretical expectation in some grids in the western United States, the north Great Plains and the eastern coastal

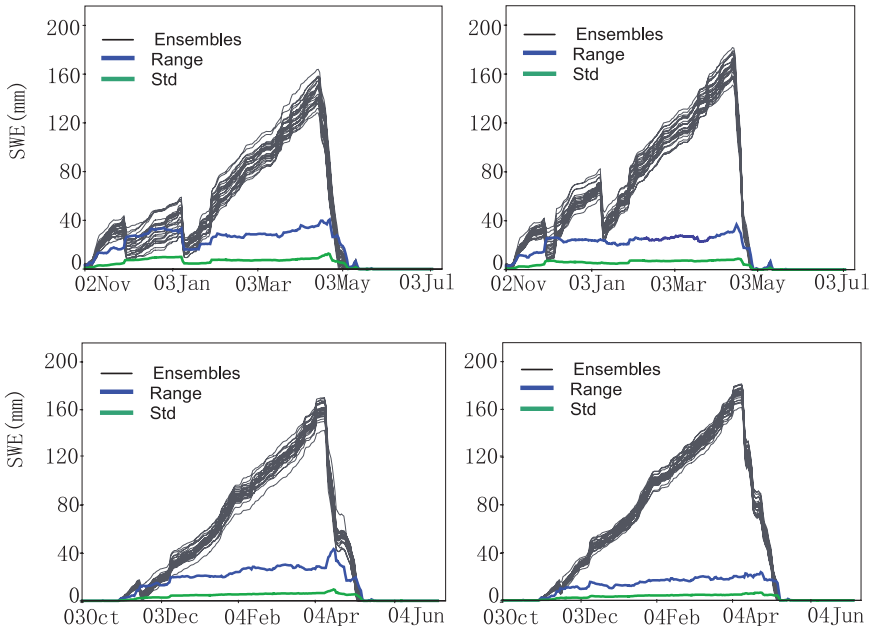

Figure 9. Ensemble simulations of SWE and their error statistics at a grid in the boreal forest region. Left panels show the open loop run; right panels show the EnKF run. Upper panels are for 2002–2003; lower panels are for 2003–2004. Ensemble simulations are represented by gray curves, the range (difference between the maximal ensemble value and the minimal ensemble value) of ensemble by the blue curve, and the standard deviation of ensemble by the green curve.

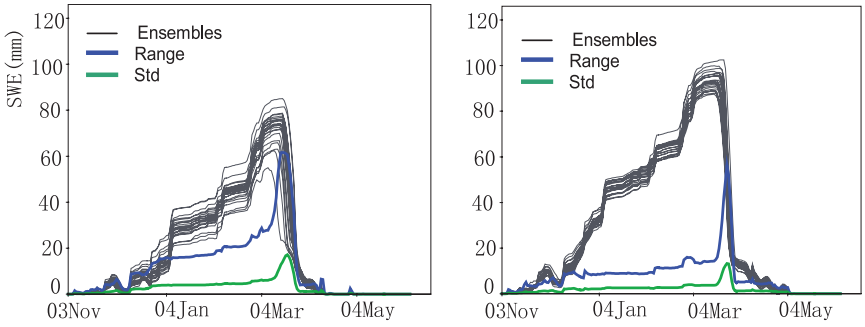

Figure 10. Ensemble simulations of SWE and their error statistics at the grid in the mountainous region. Left panels show the open loop run; right panels show the EnKF run. Ensemble simulations are represented by gray curves, the range (difference between the maximal ensemble value and the minimal ensemble value) of ensemble by the blue curve, and the standard deviation of ensemble by the green curve.

regions, but is lower than one in the northern tundra area. The prescribed forcing errors may be underestimated in the regions where this statistic is larger than one, while in the regions where this statistic is lower than 1.0, the forcing errors may be overestimated. This implication is intuitively reasonable considering that in the middle latitude region where the ground temperature often fluctuates around the freezing point in the cold season, and in the mountainous region where the precipitation is difficult to observe, the atmospheric forcing errors are easily underestimated. Some methods can be applied to tackle the above problem, for example, using ground observations to derive reliable error estimation through the comparisons with the model forcings [e.g., *Reichle et al.*, 2002], or using observed land variables (e.g., SWE) to calibrate the error statistics. These approaches treat the error covariance as a tunable parameter in the data assimilation system. However, they are suitable for applications with more atmosphere or land surface measurements.

6. Concluding Remarks

[34] This research investigates the feasibility of applying an EnKF data assimilation approach with a highly complex land surface model (CLM) for optimally estimating continental-scale snow water equivalent with MODIS observed SCF. A newly developed observational operator based on snow density is applied. Through this operator and the sequential assimilation scheme, the useful information contained in the MODIS snow cover data are projected into the CLM propagated ensemble SWE fields. An evaluation of the results for North America indicates the validity of the proposed method, which depends on ground snow measure-

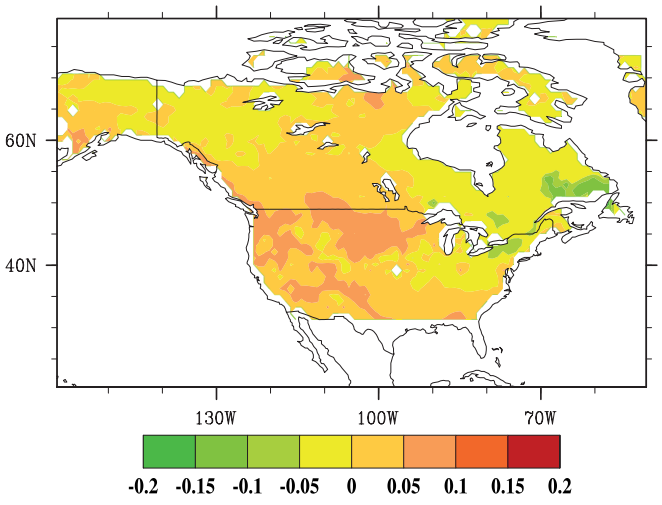

Figure 11. Spatial distribution of the average of the innovation (difference between observation and simulation) mean for the winter season in the 2002–2003 simulation (December 2002 to April 2003). This value is significantly larger than its theoretical expectation, 0, in some grids in the western United States and the northern Great Plains, representing that the model system has low bias there. In contrast, the value is lower than 0 in northeast North America, representing that the model system has high bias there.

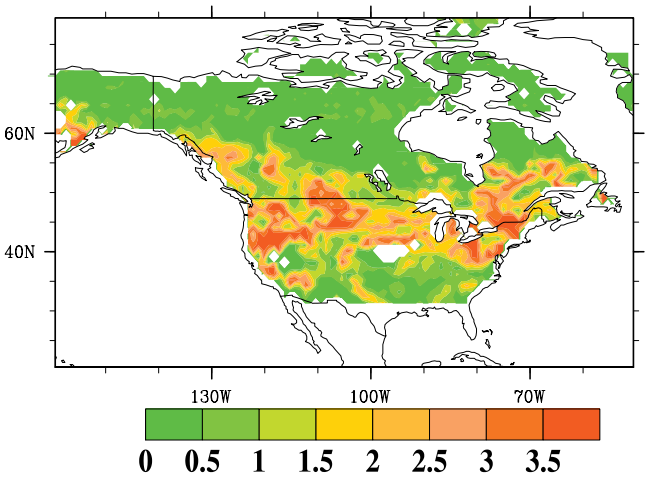

Figure 12. Spatial distribution of the mean of normalized innovation variance (equation (7) for the winter season of December 2002 to April 2003). This value is significantly larger than its theoretical expectation, 1, in some grids in the western United States, the northern Great Plains, and the eastern coastal regions. In contrast, the value is lower than 1 in the northern tundra area.

ments and independent satellite observations. In addition, the multiyear regridded data set is used to provide a reliable reference to evaluate the spatial differences between the EnKF and open loop simulations. Analyses of the filter performance further suggests that the EnKF is suitable for resolving uncertainties associated with the large-scale snow simulation system in distinct landscape and climatic zones. This work also characterizes some key issues in the EnKF snow estimation framework, such as the system bias and model error misrepresentation. It provides the spatial distributions of related statistics useful for characterizing the quality of the data assimilation system. The method could be improved by better quantification of the errors in the modeling system including its mean value (bias) and variance.

[35] **Acknowledgments.** This work is funded by NASA grants NAG5-10209 and NAG5-12577. Matthew Rodell is thanked for providing GLDAS forcing data. MODIS and AMSR-E snow data are provided by National Snow and Ice Data Center.

References

Anderson, E. A. (1976), A point energy and mass balance model of a snow cover, *NOAA Tech. Rep. NMFS*, *19*, 150 pp.

Andreadis, K. M., and D. P. Lettenmaier (2006), Assimilating remotely sensed snow observations into a macroscale hydrology model, *Adv. Water Resour.*, *29*, 872–886.

Barnett, T. P., L. Dumenil, U. Schlese, E. Roechner, and M. Latif (1989), The effect of Eurasian snow cover on regional and global climate variations, *J. Atmos. Sci.*, *46*, 661–685.

Bonan, K., W. Oleson, M. Vertenstein, S. Levis, X. B. Zeng, Y. J. Dai, R. E. Dickinson, and Z. L. Yang (2002), The land surface climatology of the community land model coupled to the NCAR community climate model, *J. Clim.*, *15*, 3123–3149.

Brown, R. D., B. Brasnett, and D. Robinson (2003), Gridded North American monthly snow depth and snow water equivalent for GCM evaluation, *Atmos. Ocean*, *41*(1), 1–14.

Brubaker, K. L., M. Jasinski, A. T. Chang, and E. Josberger (2001), Interpolating sparse surface measurements for calibration and validation of satellite-derived snow water equivalent in Russian Siberia, *IAHS Publ.*, *267*, 93–98.

Brubaker, K. L., R. T. Pinker, and E. Deviatova (2005), Evaluation and comparison of MODIS and IMS snow-cover estimates for the continental United States using station data, *J. Hydrometeorol.*, *6*, 1002–1017.

Burgers, G., P. J. van Leeuwen, and G. Evensen (1998), Analysis scheme in the ensemble Kalman filter, *Mon. Weather Rev.*, *126*, 1719–1724.

Clark, M. P., et al. (2006), Assimilation of snow covered area information into hydrologic and land-surface models, *Adv. Water Resour.*, *29*, 1209–1221.

Crow, W. T. (2003), Correcting land surface model predictions for the impact of temporally sparse rainfall rate measurements using an ensemble Kalman filter and surface brightness temperature observations, *J. Hydrometeorol.*, *4*, 960–973.

Crow, W. T., and E. V. Loon (2006), Impact of incorrect model error assumptions on the sequential assimilation of remotely sensed surface soil moisture, *J. Hydrometeorol.*, *7*, 421–433.

Dee, D. P. (1995), On-line estimation of error covariance parameters for atmospheric data assimilation, *Mon. Weather Rev.*, *123*, 1128–1145.

Dingman, S. L. (2002), *Physical Hydrology*, 2nd ed., Prentice-Hall, Upper Saddle River, N. J.

Dong, J., J. P. Walker, and P. R. Houser (2005), Factors affecting remotely sensed snow water equivalent uncertainty (2005), *Remote Sens. Environ.*, *97*, 68–82.

Dong, J., J. P. Walker, P. R. Houser, and C. Sun (2007), Scanning multichannel microwave radiometer snow water equivalent assimilation, *J. Geophys. Res.*,*112*,D07108, doi:10.1029/2006JD007209.

Durand, M., and S. A. Margulis (2006), Feasibility test of multifrequency radiometric data assimilation to estimate snow water equivalent, *J. Hydrometeorol.*, *7*, 443–457.

Durand, M., and S. A. Margulis (2007), Correcting first-order errors in snow water equivalent estimates using a multifrequency, multiscale radiometric data assimilation scheme, *J. Geophys. Res.*,*112*, D13121, doi:10.1029/2006JD008067.

Epstein, E. S. (1969), Stochastic dynamic prediction, *Tellus, Ser. A*, *21*, 739–759.

Evensen, G. (1994), Sequential data assimilation with a nonlinear QG model using Monte Carlo methods to forecast error statistics, *J. Geophys. Res.*, *99*, 10,143–10,162.

Evensen, G. (2003), The ensemble Kalman filter: Theoretical formulation and practical implementation, *Ocean Dyn.*, *53*, 343–367.

Foster, J. L., C. J. Sun, J. P. Walker, R. Kelly, A. Chang, J. R. Dong, and H. Powell (2005), Quantifying the uncertainty in passive microwave snow water equivalent observations, *Remote Sens. Environ.*, *94*, 187–203.

Gong, G., D. Entekhabi, and J. Cohen (2003), Modeled Northern Hemisphere winter climate response to realistic Siberian SNOW ANOMALIES, *J. Clim.*, *16*, 3917–3931.

Grody, N. C., and A. N. Basist (1996), Global identification of snowcover using SSM/I measurements, *IEEE Trans. Geosci. Remote Sens.*, *34*(1), 237–249.

Hall, D. K., and G. A. Riggs (2007), Accuracy assessment of the MODIS snow products, *Hydrol. Processes*, *21*, 1534–1547.

Hall, D. K., G. A. Riggs, and V. V. Salomonson (1995), Development of methods for mapping global snow cover using moderate resolution imaging spectroradiometer data, *Remote Sens. Environ.*, *54*, 127–140.

Hall, D. K., et al. (2002), MODIS snow-cover products, *Remote Sens. Environ.*, *83*, 181–194.

Hamill, T. M. (2006), Ensemble-based atmospheric data assimilation, in *Predictability of Weather and Climate*, edited by T. Palmer and R. Hagedorn, pp. 124–156, Cambridge Univ. Press, New York.

Houser, P. R., et al. (1998), Integration of soil moisture remote sensing and hydrologic modeling using data assimilation, *Water Resour. Res.*, *34*, 3405–3420.

Klein, A. G., and A. C. Barnett (2003), Validation of daily MODIS snow maps of the Upper Rio Grande River Basin for the 2000–2001 snow year, *Remote Sens. Environ.*, *86*, 162–176.

Liston, G. E. (2004), Representing subgrid snow cover heterogeneities in regional and global models, *J. Clim.*, *17*, 1381–1397.

Luce, C. H., and D. G. Tarboton (1999), Sub-grid parameterization of snow distribution for an energy and mass balance snow cover model, *Hydrol. Processes*, *13*, 1921–1933.

Luce, C. H., and D. G. Tarboton (2004), The application of depletion curves for parameterization of sub-grid variability of snow, *Hydrol. Processes*, *18*, 1409–1422.

Margulis, S. A., D. McLaughlin, D. Entekhabi, and S. Dunne (2002), Land data assimilation and estimation of soil moisture using measurements from the Southern Great Plains 1997 Field Experiment, *Water Resour. Res.*, *38*(12),1299, doi:10.1029/2001WR001114.

Markus, T., D. C. Powell, and J. R. Wang (2006), Sensitivity of passive microwave snow depth retrievals to weather effects and snow evolution, *IEEE Trans. Geosci. Remote Sens.*, *44*(1), 68–77.

McLaughlin, D. B. (2002), An integrated approach to hydrologic data assimilation: Interpolation, smoothing, and filtering, *Adv. Water Resour.*, *25*, 1275–1286.

Meteorological Service of Canada (2000), *Canadian Snow Data CD: Daily Snow Depth and Snow Water Equivalent* [CD-ROM],Downsview, Ont., Canada. (Available at http://www.ccin.ca/datasets/snowcd/docs/1999/Readme.htm)

Mote, T., A. Grundstein, D. Leathers, and D. Robinson (2003), A comparison of modeled, remotely sensed, and measured snow water equivalent in the northern Great Plains, *Water Resour. Res.*, *39*(8),1209, doi:10.1029/2002WR001782.

Nijssen, B., and D. P. Lettenmaier (2004), Effect of precipitation sampling error on simulated hydrological fluxes and states: Anticipating the Global Precipitation Measurement satellites, *J. Geophys. Res.*, *109*, D02103, doi:10.1029/2003JD003497.

Niu, G.-Y., and Z.-L. Yang (2007), An observation-based formulation of snow cover fraction and its evaluation over large North American river basins, *J. Geophys. Res.*, *112*, D21101, doi:10.1029/2007JD008674.

Niu, G.-Y., Z-.L. Yang, R. E. Dickinson, and L. E. Gulden (2005), A simple TOPMODEL-based runoff parameterization (SIMTOP) for use in global climate models, *J. Geophys. Res.*, *110*, D21106, doi:10.1029/2005JD006111.

Oleson, K. W., et al. (2004), Technical description of the Community Land Model (CLM), *NCAR Tech. Note NCAR/TN-461+STR*, 173 pp., Natl. Cent. for Atmos. Res.,Boulder, Colo.

Reichle, R. H., and R. D. Koster (2003), Assessing the impact of horizontal error correlations in background fields on soil moisture estimation, *J. Hydrometeorol.*, *4*, 1229–1242.

Reichle, R. H., and R. D. Koster (2004), Bias reduction in short records of satellite soil moisture, *Geophys. Res. Lett.*, *31*, L19501, doi:10.1029/2004GL020938.

Reichle, R. H., D. B. McLaughlin, and D. Entekhabi (2002), Hydrologic data assimilation with the ensemble Kalman filter, *Mon. Weather Rev.*, *130*, 103–114.

Rodell, M., and P. R. Houser (2004), Updating a land surface model with MODIS-derived snow cover, *J. Hydrometeorol.*, *5*, 1064–1075.

Rodell, M., et al. (2004), The global land data assimilation system, *Bull. Am. Meteorol. Soc.*, *85*, 381–394.

Simic, A., R. Fernandes, R. Brown, P. Romanov, W. Park, and D. K. Hall (2004), Validation of VEGETATION, MODIS, and GEOS + SSM/I snow-cover products over Canada based on surface snow depth observations, *Hydrol. Processes*, *18*, 1089–1104.

Slater, A. G., and M. P. Clark (2006), Snow data assimilation via an ensemble Kalman filter, *J. Hydrometeorol.*, *7*, 3–22.

Tedesco, M., E. J. Kim, A. W. England, R. de Roo, and J. P. Hardy (2006), Brightness temperatures of snow melting/refreezing cycles: Observations and modeling using a multilayer dense medium theory-based model, *IEEE Trans. Geosci. Remote Sens.*, *44*(12), 3563–3573.

Yang, F., A. Kumar, W. Wang, H. H. Juang, and M. Kanamitsu (2001), Snow-albedo feedback and seasonal climate variability over North America, *J. Clim.*, *14*, 4245–4248.

Yang, Z.-L., and G.-Y. Niu (2003), The Versatile Integrator of Surface and Atmosphere Processes (VISA) part 1: Model description, *Global Planet. Change*, *38*, 175–189.

Yang, Z.-L., R. E. Dickinson, A. Robock, and K. Y. Vinnikov (1997), Validation of the snow sub-model of the biosphere-atmosphere transfer scheme with Russian snow cover and meteorological observational data, *J. Clim.*, *10*, 353–373.

R. E. Dickinson, Department of Earth and Atmospheric Sciences, Georgia Institute of Technology, 311 Ferst Drive, Atlanta, GA 30332-0340, USA.

G.-Y. Niu, H. Su, and Z.-L. Yang, Department of Geological Sciences, The John A. and Katherine G. Jackson School of Geosciences, University of Texas at Austin, C1100, Austin, TX 78712, USA. (liang@mail.utexas.edu)